Electromagnetic Computations of High Speed Single-Sided Linear Induction Machines Using a Modified Method

Mehran Mirzaei †and Seyed Ehsan Abdollahi †
† Department of Electrical Engineering, Amirkabir University of Technology, Iran
Tel: +98(0)21 64543536 – e-mail: mehranamirzaei@yahoo.com

Topics: 11, 71

1. Introduction

Linear induction machines (LIMs) are suitable propulsion systems for high-speed light railways (e.g. Tokyo, Kobe, Kuala Lumpur, Toronto, Vancouver, and Detroit), elevator propulsions, elevator door openers and roller coasters. Thus, analysis and optimization of these machines thoroughly should be performed.

Analysis of solid secondary high speed linear induction machines is time consuming and requires large computer memory because of end effects that cause large region to be analyzed [1]. Saturation and unstable numerical analysis due to cell Reynolds number increase at high speeds, also complicates the analysis. In addition, in proposing a design optimization of the machine, a fast and stable analysis is important. In recent years, a number of methods such as finite element and analytical methods have been proposed for analysis of solid secondary linear induction machines [1]-[2]. Finite element method (FEM) is precise, but it has the disadvantages of giving unstable response and being time consuming due to high cell Reynolds number. One even can argue that FEM is not economical for high speed linear induction machines analysis. Analytical methods do not have those shortcomings and estimate magnetic fields in the secondary and also in the air gap with high precision, but cannot consider the effects of teeth and slots directly.

The application of combined analytical and finite element methods in the air gap of electrical machines was first discussed in [3] - [4]. The major advantage of this method is that the sensitivity of the finite element solution to the mesh in the air gap region can be eliminated. Numerical techniques based on this idea are seen to be effective to achieve higher accuracy in air gap field prediction.

In this paper, an enhanced method for analysis of high speed single-sided linear induction machines (LIMs) with solid secondary is developed. The longitudinal end effect, transverse edge effect, and back-iron saturation are considered in the proposed analysis. A computationally efficient combined finite element and analytical method for simulating the performance of high speed linear induction machines is presented. It is shown that the coupled two dimensional analytical and finite element methods can be used for electromagnetic computations of linear induction machines with solid secondary. The calculated thrust forces are in good agreement with the test results. Also, it is shown that the proposed method can provide stable computational predictions of magnetic field problems, and can be used as a design and analysis tool for linear induction machines.

2. Modelling

Fig. 1 shows the three dimensional view of the single-sided linear induction motor. The secondary solid iron width is equal to the primary core width. The secondary is double layer.

Because of two dimensional analysis, the transverse effect or the third dimension must be considered. According to Fig. 1, the transverse edge effect in the solid secondary is accounted for by the Russel-Norsworthy factors [1] which modify the secondary conductivities to:

$$\sigma'_{Al} = K_{Al}\sigma_{Al}$$
$$K_{Al} = 1 - \frac{\tanh(kWp)}{kWp\left(1 + \tanh(kWp)\tanh(k(Ws - Wp))\right)} \quad (1)$$

$$\sigma'_{Fe} = K_{Fe}\sigma_{Fe}$$
$$K_{Fe} = 1 - \frac{\tanh(kWp)}{kWp} \quad , \quad k = \frac{\pi}{2\tau} \quad (2)$$

Where, σ_{Al}, σ_{Fe}, and τ are the secondary aluminum cap conductivity, secondary back iron conductivity and the pole pitch, respectively.

The two dimensional view of the proposed model is shown in Fig. 2. In the figure, a segment of the analysis region is depicted. The analytical method is used in the solid secondary region, while the FEM is applied to obtain the electromagnetic fields in the stator core. In the air-gap, both methods are implemented using the corresponding boundary conditions.

A symmetric time-harmonic current system is considered. The governing differential equations are as follows:

$$\nabla \times H = J,\ B = \mu H,\ \nabla \times A = B$$
$$\nabla \times E = -\frac{dB}{dt},\ J = \sigma E \quad (3)$$
$$\nabla \times \frac{1}{\mu}\nabla \times A = -\sigma\frac{dA}{dt} = -\sigma(j\omega A + U_x\frac{\partial A}{\partial x})$$

Where, B, J, A, U_x and ω are the magnetic flux density, current density, magnetic vector potential, linear velocity of secondary and angular frequency respectively. Variables σ and μ are the electrical conductivity and the magnetic permeability.

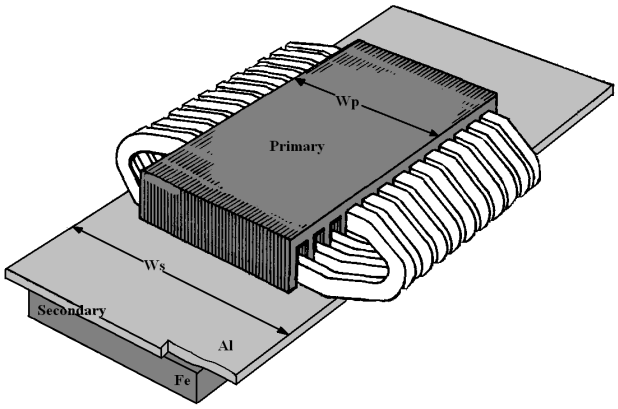

Figure 1: Linear induction machine with solid secondary

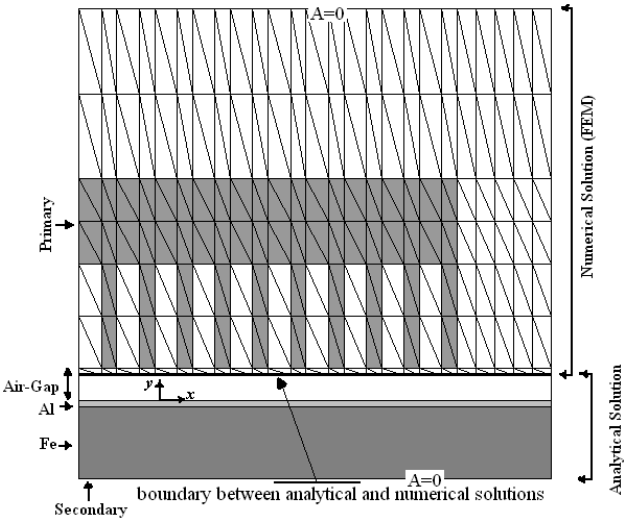

Figure 2: The proposed two dimensional model of linear solid rotor induction machine

2.1. Finite Element Method

According to Fig. 2, the primary core and surrounding regions are meshed by triangular finite elements. In this paper, the Galerkin method can be stated as:

$$\iint \frac{1}{\mu}\left[\frac{\partial N}{\partial x}\frac{\partial \mathrm{A}}{\partial x}+\frac{\partial N}{\partial y}\frac{\partial \mathrm{A}}{\partial y}\right]\mathrm{d}x\mathrm{d}y - \iint JN\mathrm{d}x\mathrm{d}y - \oint_C \frac{1}{\mu}N\frac{\partial \mathrm{A}}{\partial \hat{n}}\mathrm{d}C = 0 \tag{4}$$

is used, where N, C, and $\hat{n}$ are the shape functions, the boundary and a unit outward vector normal to the boundary respectively. The resulting system of equation is rewritten in matrix form as:

$$\begin{bmatrix} S_{11} & S_{12} \\ S_{21} & S_{22} \end{bmatrix}\begin{Bmatrix} \mathrm{A}_1 \\ \mathrm{A}_2 \end{Bmatrix} + \begin{Bmatrix} 0 \\ R \end{Bmatrix} = \begin{Bmatrix} F \\ 0 \end{Bmatrix} \tag{5}$$

Where, the subscripts 1 and 2 stand for the interior and boundary nodes, respectively. The matrix [S] and vector $\{F\}$ are the system matrix and source function from the FEM. The vector R is:

$$R = \{R_1, R_2, ..., R_{M_B}\} \tag{6}$$

Where, M_B is the number of nodes on the boundary between analytical and numerical solutions. The R_i are obtained as follows:

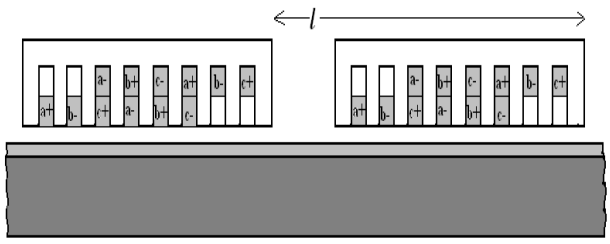

Figure 3: Mathematical model in longitudinal direction

$$R_i = -\int_{x_{i-1}}^{x_{i+1}} N_i \mathrm{H}_x \mathrm{d}x \tag{7}$$

Where, N_i are shape functions, x_i are x coordinates of nodes in the boundary between analytical and numerical solutions and H_x is the tangential component of the magnetic field intensity that will be computed by analytical solution [5].

2.2. Analytical Method

The electromagnetic fields in the secondary and a part of air gap are computed by space harmonic method [6].

According To Fig. 3, it is assumed that the motor structure is repeated in longitudinal direction. In doing so, one must, however, insert gap according to Fig. 3 between the individual primary members. These gaps are necessary because, at high speeds, the magnetic field leaks out of primary core as a result of end effects.

The analytical solutions of (3) in three regions are as follows:

$$^{k}\mathrm{A} = \sum_{n=-M_h}^{M_h} {}^{k}C_n(\cosh({}^{k}\lambda_n y) + {}^{k}C'_n \sinh({}^{k}\lambda_n y)) \times \exp(j(\omega t - \frac{2\pi n}{l}x)), \quad n = ...,-3,-2,-1,1,2,3... \tag{8}$$

Air gap ($k = 1$)

$$^{1}\lambda_n = \left|\frac{2\pi n}{l}\right|$$

Aluminum($k = 2$)

$$^{2}\lambda_n = \sqrt{(\frac{2\pi n}{l})^2 + j\sigma'_{Al}\mu_0(\omega + \mathrm{U_x}\frac{2\pi n}{l})} \tag{9}$$

Iron($k = 3$)

$$^{3}\lambda_n = \sqrt{(\frac{2\pi n}{l})^2 + j\sigma'_{Fe}\mu_{Fe}\mu_0(\omega + \mathrm{U_x}\frac{2\pi n}{l})}$$

Where, $^{1,2,3}C_n$ and $^{1,2,3}C'_n$ are constants that obtained from related boundary conditions between different regions in analytical solution and FEM solution. l is the repeating period of the linear induction machine structure (Fig. 3), μ_0 and μ_{Fe} are vacuum permeability and effective relative permeability of the secondary iron, respectively. M_h and n are maximum number of considered harmonics and harmonics order, respectively.

In a saturable ferromagnetic material, sinusoidal varying magnetic field strength creates a non-sinusoidal magnetic flux density. The amplitude of the flux density can be numerically defined with the DC-magnetization curve of the material. Only the fundamental amplitude

which is considerably higher than the real maximum value is considered and the harmonics may be ignored in the analysis of the active power because only waves with the same frequency create power. So, the saturation dependent fundamental permeability of the material is defined. The fundamental amplitude of the Fourier series of the flux density is obtained by a numerical integration [7].

The effective relative permeability for entire secondary iron is obtained through an iterative procedure using the chord method [8]. Initially, a constant value for relative permeability of iron is considered then the value updated to correspond to the ones given by the B1-H curve using multipliers known as relaxation factors. Because of high skin effect in iron, only x component of field in ferromagnetic region is considered for permeability computation.

$$\mu_{Fe}\mu_0 = \frac{\hat{\mathrm{B}}_1}{\hat{\mathrm{H}}} \quad , \; {}^3\mathrm{H}_x = \hat{\mathrm{H}}\sin(\omega t) \tag{10}$$

$$\hat{\mathrm{B}}_1 = \frac{2}{\pi}\int_0^{\pi} {}^3\mathrm{B}_x(\omega t)\sin(\omega t)\mathrm{d}(\omega t)$$

$$\mu_{Fe}(\text{new}) = \mu_{Fe}(\text{old}) + \beta(\mu_{Fe}(\text{new}) - \mu_{Fe}(\text{old})) \tag{11}$$

2.3. Coupling Scheme

Coupling between analytical and FEM solutions is done through the following boundary conditions:

$$\begin{aligned} &\mathrm{H}_x(\text{FEM}) = \mathrm{H}_x(\text{analytical}) \\ &\mathrm{A}(\text{FEM}) = \mathrm{A}(\text{analytical}) \end{aligned} \tag{12}$$

Magnetic vector potential and magnetic field intensity in the air gap that calculated using analytical solution are obtained as follows:

$$\begin{aligned} {}^1\mathrm{A}(x,y) = &\sum_{n=-M_h}^{M_h} {}^1C_n(\cosh({}^1\lambda_n y) + \\ &{}^1C'_n \sinh({}^1\lambda_n y)) \times \exp(j(\omega t - \frac{2\pi n}{l}x)) \\ {}^1\mathrm{H}(x,y) = &\sum_{n=-M_h}^{M_h} {}^1\lambda_n \, {}^1C_n(\sinh({}^1\lambda_n y) + \\ &{}^1C'_n \cosh({}^1\lambda_n y)) \times \exp(j(\omega t - \frac{2\pi n}{l}x)) \end{aligned} \tag{13}$$

According to Fig. 4, the shape function in (7) that is necessary for coupling procedure is given by:

$$N_i = \begin{cases} \dfrac{x - x_{i-1}}{x_i - x_{i-1}} & \text{if} \quad x_{i-1} \le x \le x_i \\ \dfrac{x - x_{i+1}}{x_i - x_{i+1}} & \text{if} \quad x_i \le x \le x_{i+1} \\ 0 & \text{if} \quad x \le x_{i-1} \\ 0 & \text{if} \quad x \ge x_{i+1} \end{cases} \tag{14}$$

By applying (12) between analytical and numerical solutions and using (14) in (7), the complete equations of the full structure of linear induction machine are obtained.

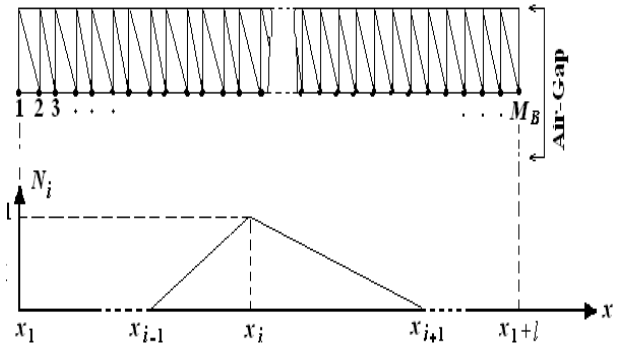

Figure 4: Definition of shape function

The unknown variables are the magnetic vector potential of finite element nodes and constants of air gap magnetic vector potentials of analytical solution [9].

3. Simulation

A high speed linear induction motor is considered for the simulation study. The design data of the considered single sided linear induction motor (GE) is given in [1]. The simulation is performed with constant current source of 200 (A) and 60 (Hz) frequency. Magnetic characteristic of secondary iron is shown in Fig. 5. The figure depicts DC magnetizing curve and B_1-H curve related to the fundamental component of magnetic flux density.

The permeability of solid iron secondary can be approximated by the following equation for simulation [10]:

$$\mu_{Fe}\mu_0 = \frac{1}{\mathrm{k}_1 + \mathrm{k}_2\mathrm{B}_1^{\,8} + \mathrm{k}_3\mathrm{B}_1^{\,10}} \tag{14}$$

$$\mathrm{k}_1 = 632.2, \quad \mathrm{k}_2 = 8.93, \quad \mathrm{k}_3 = -0.652$$

Where, B_1 is the x component of magnetic flux density amplitude in secondary iron. At zero speed, the magnetic flux density in the boundary between iron and aluminum is considered and because of increasing magnetic flux penetration in iron with speed increasing, the magnetic flux density in inner part of secondary iron is considered for effective permeability computation.

In this simulation, for obtaining better results at high speeds with high end effects, the number of nodes M_B in the common boundary should be equal to two times the maximum harmonics number $2M_h$. The total length of the model for simulation and end effects consideration is considered two times the longitudinal motor length. The number of nodes M_B equal to 176 is sufficient.

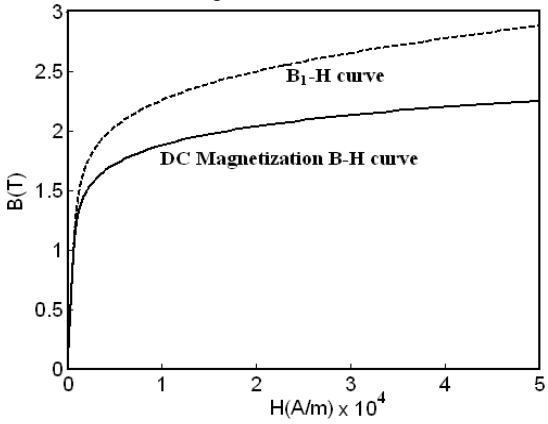

Figure 5: Magnetic characteristic of secondary iron

Relaxation factor equals 0.1 yields good convergence in nonlinear solution. For proving the accuracy and capability of the presented method, the calculated thrust forces and experimental ones of the high speed linear induction motor are compared in Fig. 6.

It is shown that the proposed method has high ability in thrust force calculation of linear induction machines. Fig. 7 shows the effective relative permeability variations of the secondary iron with speed. The magnetic flux distribution in the motor structure at zero speed is shown in Fig. 8.

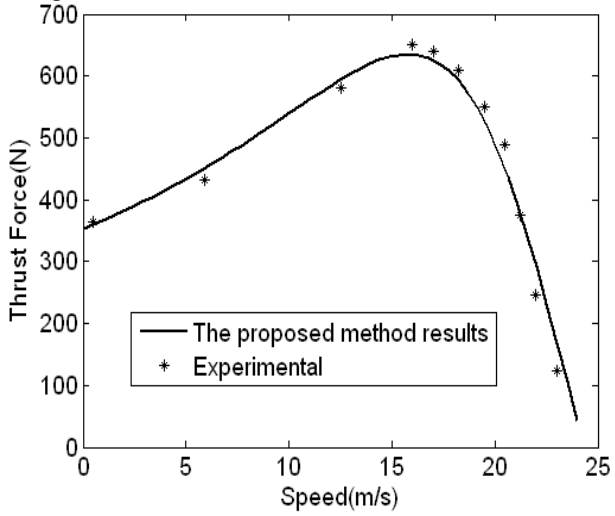

Figure 6: Comparison between computed results and experimental ones

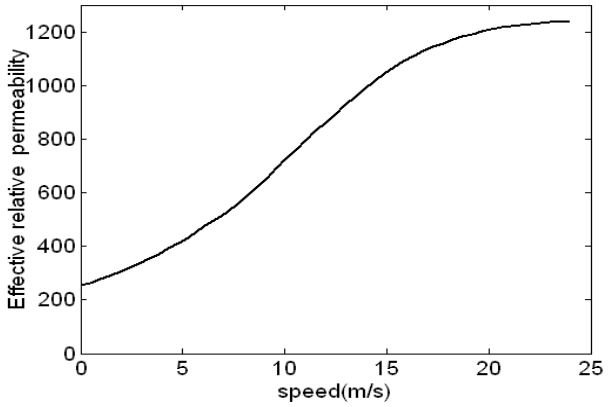

Figure 7: Effective relative permeability curve of secondary iron

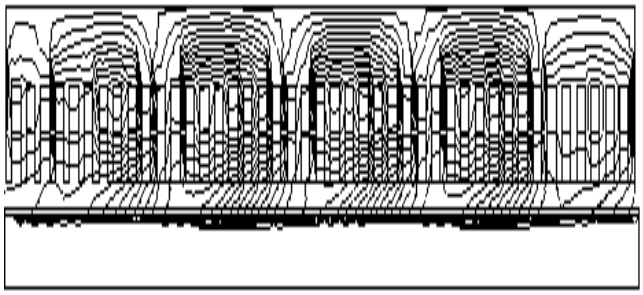

Figure 8: Magnetic flux distribution at zero speed

4. Conclusion

Using the presented method, it is possible to analyze and design high speed linear induction machines with high accuracy over a shorter time period. Optimum design of the motor using the combined method needs less memory that is important in large linear induction motors with high end effects. This method can be used for analysis of other solid moving part electromagnetic devices such as solid iron secondary linear induction machines and eddy current brakes.

References

[1] J. F. Gieras, "*Linear Induction Drives*", Clarendon Press. Oxford, , 1994

[2] T. Furukawa, K. Komiya, and I. Muta, "*An upwind Galerkin finite element analysis of linear induction motors*", IEEE Transactions on Magnetics, Vol. 26, No. 2, pp. 662-665, 1990

[3] A. A. Abdel-Razek, J. L. Coulomb, M. Feliachi, and J. C. Sabonnadiere, "*The calculation of electromagnetic torque in saturated electric machines within combined numerical and analytical solution in the field equations*", IEEE Transactions on Magnetics., Vol. 17, pp. 3250–3252, Nov. 1981.

[4] A. A. Abdel-Razek, J. L. Coulomb, M. Feliachi, and J. C.Sabonnadiere, "*Conception of an air-gap element for the dynamic analysis of the electromagnetic field in electric machines*", IEEE Transactions on Magnetics., vol. 18, pp. 655–659, Mar. 1982.

[5] R. Wang, H. Mohellebi, T. J. Flack, M. J. Kamper, J. D. Buys, and M. Feliachi, "*Two-Dimensional Cartesian Air-Gap Element (CAGE) for Dynamic Finite-Element Modeling of Electrical Machines With a Flat Air Gap*", IEEE Transactions on Magnetics, Vol. 38, No. 2, pp.1357-1360, March 2002

[6] M. Mirzaei, and M. Mirsalim, "*Evaluation of the current distribution in the secondary of a high speed linear induction motor*", in Proc. ICEM2004, Lodz, Poland

[7] J. Pyrhonen, "*The high speed induction motor: calculating the effects of solid-rotor material on machine characteristics*". Phd thesis, Lappeenranta University of Technology, Finland, 1991

[8] M.V.K. Chari, and S.J. Salon, "*Numerical Methods in Electromagnetics*", Academic Press, 2000

[9] S.J. Salon, "*Finite Element Analysis of Electrical Machines*", Kluwer Academic Publishers, 1995

[10] M.E. Zaim, "*Non-linear models for the design for solid rotor induction machines*", IEEE Transactions on Magnetics,Vol.35, No.3, pp.1310-1313, 1999